



Contents lists available at ScienceDirect

## Surface &amp; Coatings Technology

journal homepage: [www.elsevier.com/locate/surfcoat](http://www.elsevier.com/locate/surfcoat)

# Characterization of thick ceramic and cermet coatings deposited by an industrial-scale LAFAD process

V.I. Gorokhovskiy \*

Arcamac Surface Engineering, LLC, Bozeman Montana, USA

## ARTICLE INFO

## Article history:

Received 2 March 2009

Accepted in revised form 14 October 2009

Available online xxxxx

## Keywords:

Filtered cathodic arc

Multilayer coatings

Fracture resistance

LAFAD

TiN

## ABSTRACT

The unidirectional LAFAD dual-arc vapor plasma source yields 100% ionized metal vapor plasma flow and more than 50% ionized gaseous plasma in the coating chamber. The LAFAD technology deposits thick ceramic and cermet coatings with multi-elemental nanostructured architectures, nearly defect-free morphology and atomically smooth surfaces at high deposition rates. The productivity of one unidirectional LAFAD vapor plasma source integrated into an industrial-scale batch coating system ranges from 3–4  $\mu\text{m}/\text{h}$  for nitride base coatings and up to 6  $\mu\text{m}/\text{h}$  for oxi-ceramic coatings with good uniformity over large deposition areas, making it an attractive alternative to other PVD processes for a wide variety of applications. The 20  $\mu\text{m}$  to 100  $\mu\text{m}$  monolithic and Ti/TiN microlaminated LAFAD coatings exhibit low residual compressive stresses, i.e. <1.5 GPa, resulting in exceptionally good adhesive and cohesive toughness. The fracture resistance of ultra-thick LAFAD coatings vs. coating architecture will be discussed.

© 2009 Published by Elsevier B.V.

## 1. Introduction

Ionized physical vapor deposition processes are known to provide improved coating structure, morphology and functional properties [1–4]. The direct cathodic arc deposition (DCAD) process produces highly ionized vapor plasma, but suffers from the large quantity of macroparticles or droplets emitted from the evaporation target surface along with atomic neutral vapor particles and ions [2]. The filtered cathodic arc deposition (FCAD) process is able to eliminate unwanted macroparticles, droplets and most of the neutrals from the metal plasma stream generated by cathodic vacuum arc process and produce nearly 100% ionized atomically clean metal vapor plasma with a relatively high electron temperature of 3 to 5 eV. The metal ion flow produced by the FCAD process consists of multi-charged ions with large kinetic energy ranging from 40 to 200 eV [2]. The main obstacle to using conventional FCAD technology is the low productivity of this process, which restricts its usage to semiconductors, optical coatings and some ultra-thin hard coatings for bio-medical and tribological applications. On the other hand, Large Area Filtered Arc Deposition (LAFAD) technology overcomes these limitations by providing a highly productive, robust, industry-friendly process which combines the high productivity rate of conventional DCAD and magnetron sputtering sources, with the capability of generating a nearly 100% ionized metal-gaseous vapor plasma having large kinetic energy and no macroparticles, droplets, multi-atom clusters or other contaminants [1,3]. This work is dedicated to the characterization of the LAFAD process integrated into an

industrial batch coating system for the deposition of thick ceramic and cermet coatings.

## 2. Experimental

Fig. 1 shows the LAFAD-500C batch coating system layout utilizing a vacuum chamber 0.7 m in diameter by 1 m tall, equipped with a unidirectional dual arc LAFAD plasma source. The rotatable substrate turntable, 0.5 m in diameter, is installed in the center of the coating chamber and allows for single or double rotation of the substrates that are being coated. The LAFAD plasma source consists of the plasma guide chamber with baffles installed along its walls and the exit tunnel window which is 300 mm wide by 400 mm tall. Primary DCAD vapor sources equipped with cathode targets made of the same or different compositions are installed on opposite walls of the plasma guide chamber. Two pairs of deflection coils are located along the opposite walls of the plasma duct chamber for turning the plasma flows from the primary DCAD sources toward the substrates to be coated in the processing chamber. Two rastering coils are installed on the top and bottom flanges of the plasma guide chamber for rastering the filtered arc plasma flow in a vertical direction perpendicular to the plane of rotation of the substrate turntable. When the deflection/focusing coils of the filter are turned on, the metal vapor plasma flows through the plasma guide chamber into the processing chamber. When the deflection/focusing coils are turned off, an auxiliary arc discharge can be established between the primary DCAD sources and the auxiliary anode in a coating chamber; this is used for ionization and activation of the gaseous plasma environment. A detailed description of this highly versatile process can be found elsewhere [1,3,5].

\* Current address: Southwest Research Institute, San Antonio, Texas, USA.

E-mail address: [vladimir.gorokhovskiy@swri.edu](mailto:vladimir.gorokhovskiy@swri.edu).

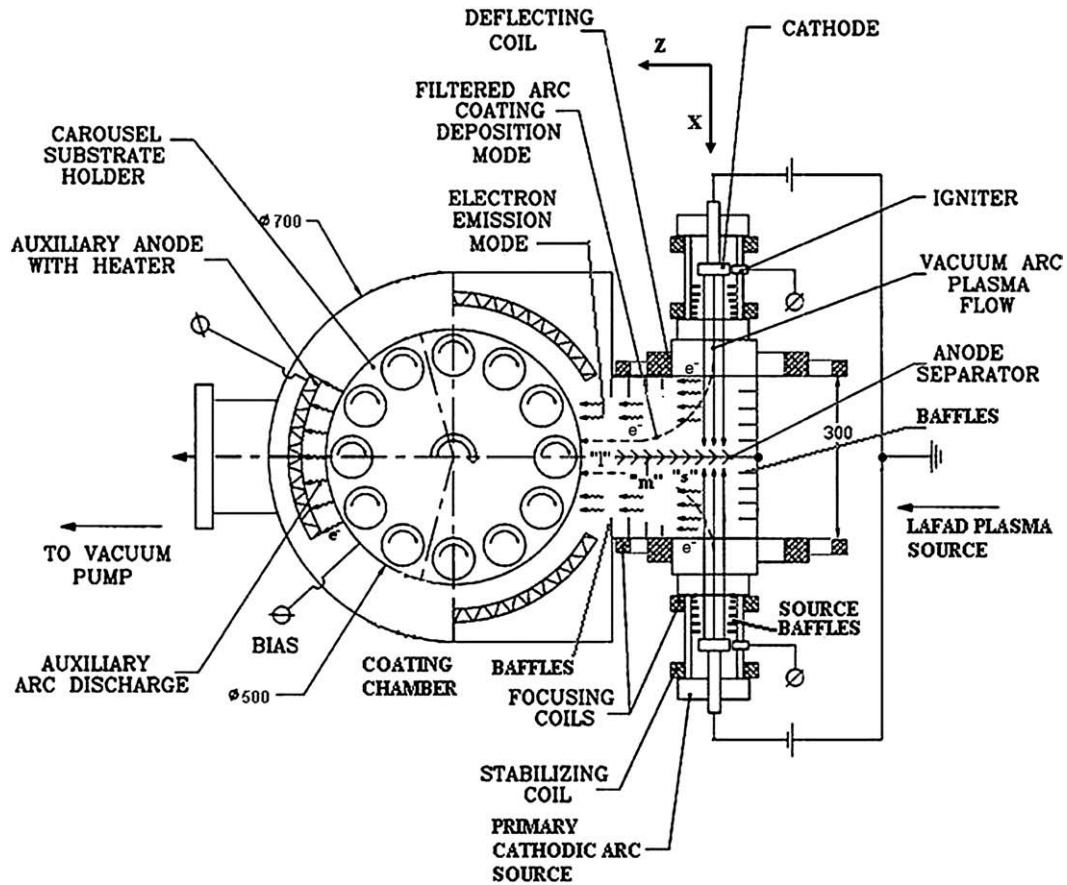


Fig. 1. Schematic illustration of the industrial-scale batch coating system with one unidirectional LAFAD metal vapor plasma source used in this study.

The typical LAFAD plasma vapor deposition trials reported in this work were performed on substrates installed on the turntable of the LAFAD batch coating system either with single rotation (SR) or with

double rotation (DR), rotating at 12 RPM. In SR mode, the substrates are rotated around the axis of the turntable with their front surface facing the chamber walls. In DR mode, substrates are subjected to double

**Table 1**  
Mechanical properties and deposition rates of thick ceramic and cermet coatings deposited by the LAFAD process on polished substrates.

Coating architecture, composition (in at.%) and sample identification (in brackets)	Primary cathodic arc current, amperes and primary target composition, at.%	Thickness, $\mu\text{m}$	Deposition rate, $\mu\text{m}/\text{h}$	Number of layers	Sublayer thickness Me/MeN, $\mu\text{m}$	Pre-deposition/post-deposition roughness RMS, $\mu\text{m}$	Hardness/elastic modulus, Gpa
TiN (A), monolithic	200	6.4+/-20% <sup>a</sup>	4+ /20%	1		0.02/0.083	34.5/461
Ti/TiN (B)	140	21.05	2.2	9	0.99/1.89	0.04/0.09	18.7/280
Ti/TiN (C)	140	20.74	2.1	8	1.18/1.73	0.03/0.23	15.8/242
Ti/TiN (D)	140	22.33	2.3	12	0.96/1.08	0.02/0.13	13.1/220
Ti/TiN (E)	140	25.30	2.5	12	0.68/1.77	0.019/0.07	19.3/301
Ti/TiN (F)	140	22.41	2.2	8	0.83/2.31	0.03/0.36	17.0/273
Ti/TiN (G)	200	50	5.2	11	2/8	0.80/0.87 <sup>b</sup>	18.7/324
TiN (H), monolithic	200	40	5	1		0.02/0.6	~35/480
TiN (I), monolithic	200	46	2.5	1		0.80/1.6 <sup>b</sup>	~35/480
TiN (J), monolithic	140	54	5	1		0.80/1.80 <sup>b</sup>	~35/480
Ti/TiN (K <sub>1</sub> )	200	50	5.2	40		0.80/0.87 <sup>b</sup>	25/415
Ti/TiN (K <sub>2</sub> )	200	30	2.5	110		0.02/0.15	25/340
{TiN (K <sub>1</sub> ) + Ti/TiN (G)}, (G K <sub>1</sub> ) 2-segments	200	100	5.2	63		0.80/0.87 <sup>b</sup>	25/415
{TiN(K <sub>1</sub> ) + Ti/TiN (I)}, (I K <sub>1</sub> ) 2-segments	200	96	5	52		0.80/1.88 <sup>b</sup>	25/415
TiN(K <sub>1</sub> ) + Ti/TiN (J), (J K <sub>1</sub> ) 2-segments	140(J)/200(K <sub>1</sub> )	46	2.5	52		0.80/1.80 <sup>b</sup>	25/415
TiAl/TiAlN (L)	200	59	5	54		0.02/0.07	30/402 <sup>b</sup>
Ti6Cr17Al23Y1048N6 (M), monolithic	140, Ti20Cr30Al48Y2	8	5	1		0.02/0.07	27/265
Ti5Cr19Al21Y1054, (N) monolithic	140, Ti20Cr30Al48Y2	12.6	6.3	1		0.02/0.06	30/290

Thickness uniformity is shown over a 20-inch diameter  $\times$  6-inch high coating area.

<sup>a</sup> Thickness distribution over a 20-inch diameter  $\times$  11-inch high coating area with vertical magnetic rastering.

<sup>b</sup> These samples were subjected to bead-blasted pre-treatment to roughness  $\sim$ 0.8  $\mu\text{m}$  RMS.

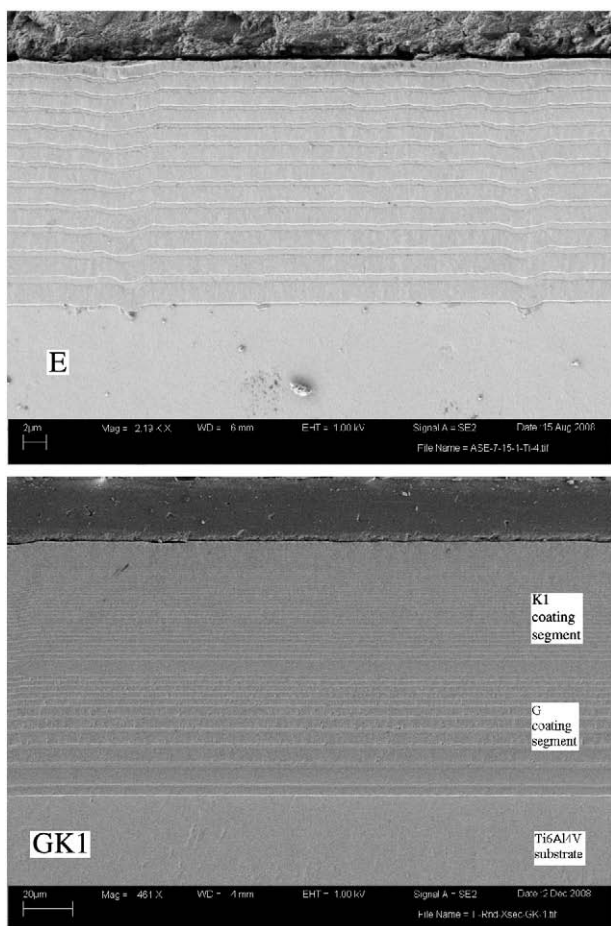


**Fig. 2.** Above: SEM image of the cross-section of a 22  $\mu\text{m}$  thick multilayer Ti/TiN coating deposited during a 10h deposition run on single rotating substrates (coating E as designated in Table 1); below: 100  $\mu\text{m}$  thick Ti/TiN two-segment nano-microlaminated coating GK<sub>1</sub> deposited in two consecutive coating runs. This coating consists of a bottom segment microlaminated G coating and a nano-laminated top K<sub>1</sub> coating as designated in Table 1.

rotation around satellite station axes as shown schematically in Fig. 1. The coating process consists of pre-heating to 350°C, 20 min of ion cleaning, and 2 min of high voltage metal ion etching; followed by coating deposition steps in a pressure range from 0.4 to 0.8 mTorr. Note that during deposition of nearly dielectric oxi-ceramic and oxi-nitride coatings, a 13.56 MHz RF generator was used as a substrate bias power supply, while for deposition of conductive coatings, an MDX-II (Advanced Energy) power supply, coupled with Sparcle-V accessory, was used as a DC bias power supply. The substrate bias during deposition of most of the conductive coatings reported in this work was  $-40$  V, while during deposition of oxiceramic and oxinitride coatings the autopolarization bias potential ranged from  $-40$  to  $-100$  V. Coatings were deposited on disk substrates made of 440A stainless steel or Ti6Al4V alloy polished to a roughness of less than 0.02  $\mu\text{m}$  RMS and on square samples made of Ti6Al4V alloy which underwent a bead blasting pre-treatment which yields a surface roughness of about 0.8  $\mu\text{m}$  RMS.

The LAFAD coatings were characterized by their basic mechanical properties: hardness, adhesion and cohesion toughness and surface profile. The thickness of thick coatings ( $>20$   $\mu\text{m}$ ) was measured by metallographic cross-section followed by SEM imaging analysis. Coating hardness and Young's modulus were measured by an MTS-XP nanoindenter with a CSM module and a Berkovich tip. SEM imaging of the micro-cross section of the Rockwell indentation was used to assess the fracture resistance of the coatings. Average coating RMS and R<sub>z</sub> roughness were measured per ASTM B46.1 with a Veeco

Dektak8 contact profilometer. Parameters for RMS measurement were as follows: 5  $\mu\text{m}$  radius stylus, 1750 $\mu\text{m}$  scan length, 250 $\mu\text{m}$  cutoff filter (waviness filter), 1 data point/ $\mu\text{m}$ . Five RMS scans were made per sample and a minimum of six samples were scanned resulting in a 30-point RMS average per unique coating type reported. The internal stress in the coatings was determined by the radius of curvature technique which compares the curvatures of bare silicon substrates vs. coated silicon substrates. The stress was then calculated by Stoney's equation. Coating compositions were analyzed by EDS, RBS, XPS and Auger techniques.

### 3. Results and discussion

Several monolithic and multilayer TiN and TiAlN based coatings with thicknesses ranging from 10 to 100  $\mu\text{m}$  were deposited by one unidirectional LAFAD vapor plasma source on substrates installed on the rotating turntable of the LAFAD coating system. The characteristic properties of these coatings and their respective deposition rates are presented in Table 1. These coatings have different architectures including monolithic I,J,M,N coatings, multilayer B,C,D,F,G coatings having a relatively large ( $>1$   $\mu\text{m}$ ) metallic sublayers followed by ceramic sublayers, which are only two or three times thicker as illustrated in the cross-section micro-image in Fig. 2 (top). Two nano-multilayer coatings K<sub>1</sub> and K<sub>2</sub> which have nanometric size metallic sublayers followed by ceramic sublayers ranging from 0.5 to 1  $\mu\text{m}$  were also deposited during separate LAFAD process runs. Coating K<sub>1</sub> has 40 bi-layers per 50  $\mu\text{m}$  of coating thickness ( i.e. 1.25  $\mu\text{m}$  per bi-layer) ; whereas coating K<sub>2</sub>, deposited with single rotation, has 110 bi-layers per coating thickness of

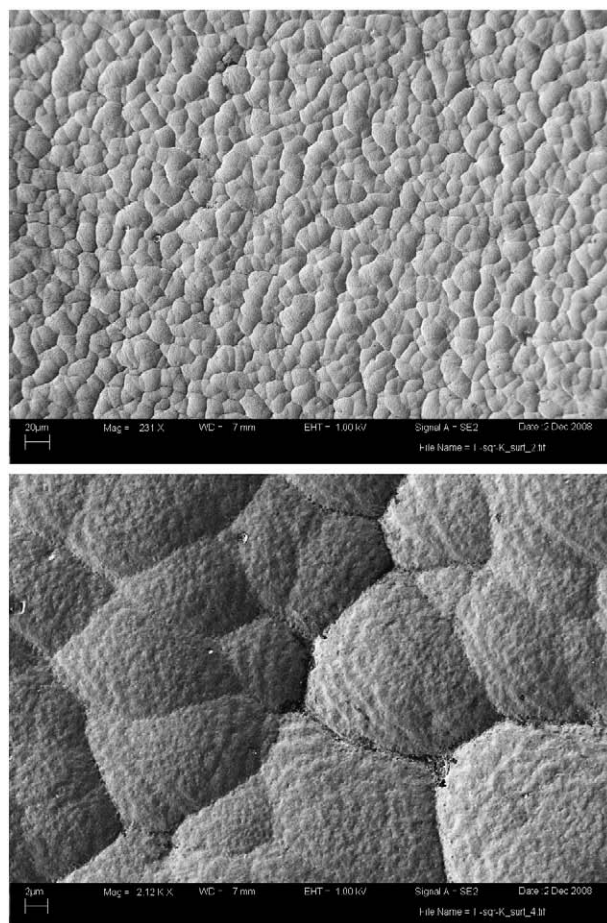


**Fig. 3.** Surface morphology of a 50  $\mu\text{m}$  thick Ti/TiN nano-laminated coating K<sub>1</sub> deposited on a bead-blasted Ti64 coupon having initial roughness of 0.8  $\mu\text{m}$  RMS (shown at two different magnifications, 231 $\times$  and 2120 $\times$ ).

30  $\mu\text{m}$  (i.e. 0.27  $\mu\text{m}$  per bi-layer). In the case of double rotation, the bi-layer thickness in coating  $K_1$  was reduced to 110 bi-layers per 12  $\mu\text{m}$  (i.e. 0.11  $\mu\text{m}$  per bi-layer). A TiAl/TiAlN nano-microlaminated coating with architecture closely resembling that of coating  $K_1$  was produced using two identical primary cathode targets having a composition of Ti30 at.% Al. In addition, two-segment coatings utilizing either monolithic IJ coatings or multilayer G coating as a bottom segment interfacing the substrate and nano-multilayer  $K_1$  top coating segment were also produced. The cross-section of a two-segment  $GK_1$  coating, deposited during two consecutive coating runs is shown in Fig. 2 (bottom). All two-segment coatings were deposited in a separate runs: the bottom segment coating in a first run followed by the top segment coating in a second run.

From Table 1 it can be seen that the deposition rate of TiN based coatings ranges from 2 to more than 5  $\mu\text{m}/\text{h}$  for TiN based coatings, depending on the arc currents of the primary DCAD sources; and exceeds 6  $\mu\text{m}/\text{h}$  for oxi-ceramic coatings, which demonstrate exceptionally high deposition rate of LAFAD process, which is comparable to, or exceeds, the productivity of conventional DCAD sources and magnetron sputtering sources for a wide variety of metal, ceramic and cermet coatings. For example, the productivity of one unidirectional LAFAD vapor plasma source integrated into an industrial-scale batch coating system ranged from 3–4  $\mu\text{m}/\text{h}$  for nitride base coatings and up to 6  $\mu\text{m}/\text{h}$  for oxiceramic coatings with good uniformity over large deposition areas, making it an attractive alternative to other PVD processes for a wide variety of applications. The LAFAD coating composition agrees closely with the composition

of the cathode targets of the primary DCAD sources even in the case of multi-elemental targets, which can be seen in coatings M and N. The metallic composition in these coatings is Ti11Cr41Al46Y2 for oxiceramic coating M and Ti11Cr40Al45Y2 for oxinitride coating N which is in good agreement with the primary target elemental composition. This means that the LAFAD process is quite effective in transferring the metal vapor elements from the evaporating cathode targets of the primary DCAD sources along the curvilinear magnetic field in the plasma guide chamber toward the substrates to be coated in the processing chamber.

The columnar morphology of thick LAFAD ceramic and cermet coatings is similar to that of coatings produced by other PVD processes such as ionized magnetron sputtering and EB-PVD [2,4], but the average size of the columnar grains is much smaller. The surface morphology and roughness of LAFAD coatings are affected by initial substrate roughness. Fig. 3 shows the morphology of the  $K_1$  coating deposited on a bead-blasted titanium sample. It can be seen that a coating deposited on a rough substrate develops a surface pattern similar to that of columnar EB-PVD and magnetron sputtered thick coatings in agreement with the Movchan–Demchishin–Thornton–Messier (MDTM) zone diagram [2], while the same 50  $\mu\text{m}$  thick coating deposited on a smooth substrate with roughness less than 0.02  $\mu\text{m}$  RMS has developed a surface roughness less than 0.2  $\mu\text{m}$  RMS as indicated in Table 1. In both cases, the coated surface shows almost no defects. The initial substrate imperfections cause a wavy distortion of the innermost layers, but the amplitude of the waviness diminishes in the layers which are further away from the substrate as can be seen

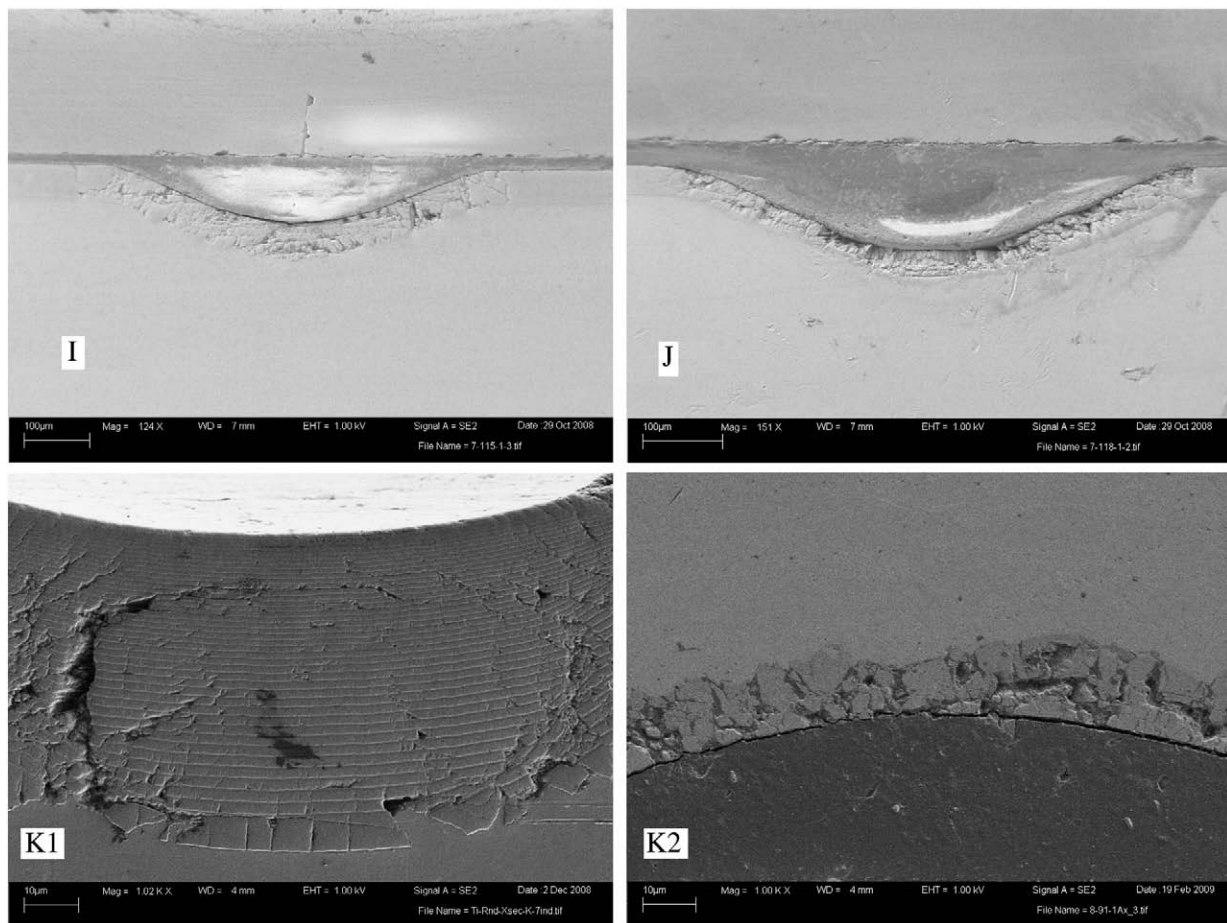


Fig. 4. SEM image of the cross-section of the Rockwell indentation of the 50  $\mu\text{m}$  thick monolithic TiN coatings and nano-microlaminated Ti/TiN coatings deposited by the LAFAD process: coating J was deposited with 140A current of the primary cathodic arc sources; coating  $K_1$  was deposited on single rotating substrate has 40 bi-layers, coating  $K_2$  was deposited on double rotating substrate has 110 bi-layers.

in Fig. 2 (top); this demonstrates the self-smoothing effect of the LAFAD process.

The 20  $\mu\text{m}$  to 100  $\mu\text{m}$  monolithic and Ti/TiN microlaminated LAFAD coatings exhibit low residual compressive stresses, i.e.  $<1.5$  GPa for coatings B–G, which can explain its exceptionally good adhesive and cohesive toughness. Low stresses in thick TiN base coatings may be explained by the role of thickness-dependent gradients of point defect density, as was recently proposed in [6]. Optimization of Ti sublayer thickness vs. TiN sublayer thickness in this microlaminated cermet coating architecture plays an important role in energy dissipation by shear deformation, which delays critical shear and tensile stress developed at the metallic/ceramic sublayers interface [5,7]. The hardness of monolithic TiN coatings reaches

35 GPa, while the hardness of the microlaminated coatings measured by the nanoindentation technique exhibits a relatively low value in the range from 18 to 20 GPa; this can be considered as a composite hardness created by the interaction of soft and ductile metallic sublayers with hard and brittle ceramic sublayers in the Ti/TiN microlaminated coating architecture. The hardness of these coatings increases when the ratio of thickness of the Ti:TiN sublayers decreases; the maximum hardness has been achieved for coatings  $K_1$  and  $K_2$  ( $>25$  GPa) and for TiAl/TiAlN coatings with similar architecture ( $>30$  GPa). The nanohardness plot indicates that the maximum hardness of TiAlN layer can exceed 40 GPa.

Qualitative fractography was conducted to assess the pattern and density of cracks developed in ultra-thick LAFAD coatings under Rockwell indentation. Cracking in ceramic in a response to stresses or strains is a way of an energy release and the density of cracks can help to assess the fracture resistance and, correspondently, the adhesion and cohesion toughness of thick LAFAD coatings. SEM images of the cross-sections of Rockwell indentations in Ti/TiN and TiAl/TiAlN multilayer and nano-microlaminated coatings as well as monolithic TiN coatings are presented in Figs. 4–6. The monolithic ultra-thick TiN coatings suffer severe fracturing in the center of the indentation where the compressive stress reaches its maximum level as shown in Fig. 4. The crack propagation pattern within the coating does not show any preferred orientation. The density of cracks is much greater in coating J, deposited at low primary cathodic arc current (140A), compared to coating I deposited at a larger primary arc current (200A). This can be explained by the higher deposition temperature of coating I which, in agreement with the MDTM zone diagram, results

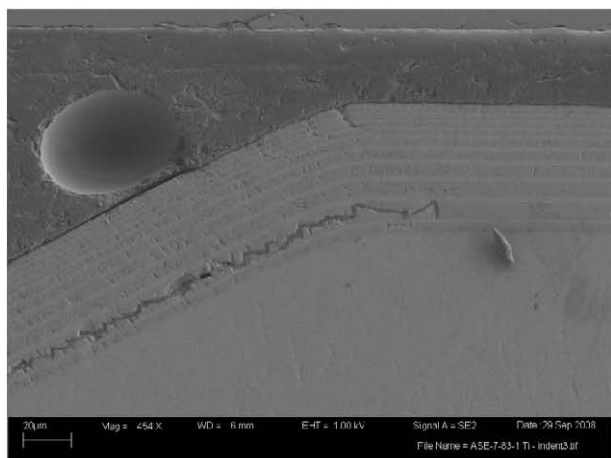
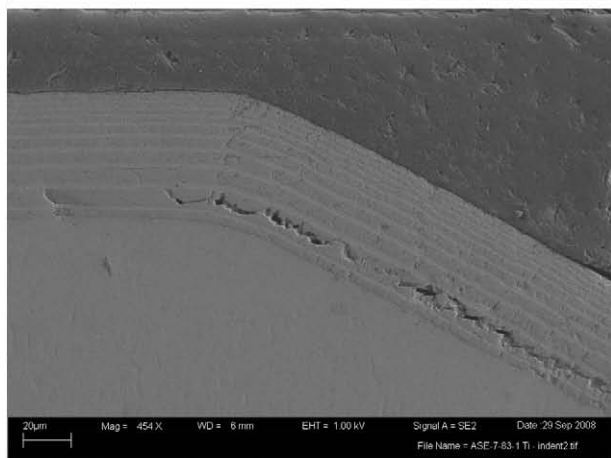
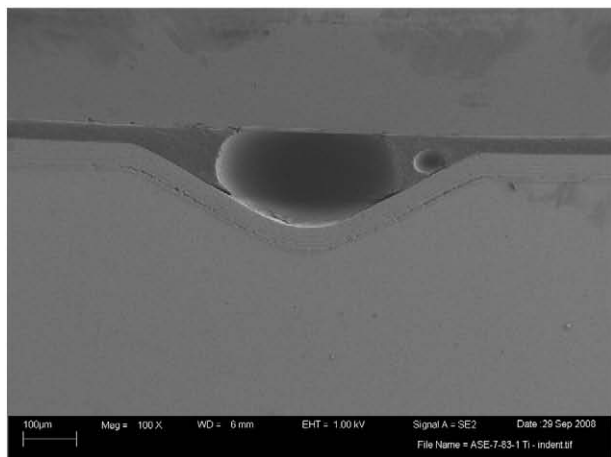


Fig. 5. SEM image of Rockwell indentation in microlaminated coating G (top) and its right side (middle) and left side (bottom) with larger magnification.

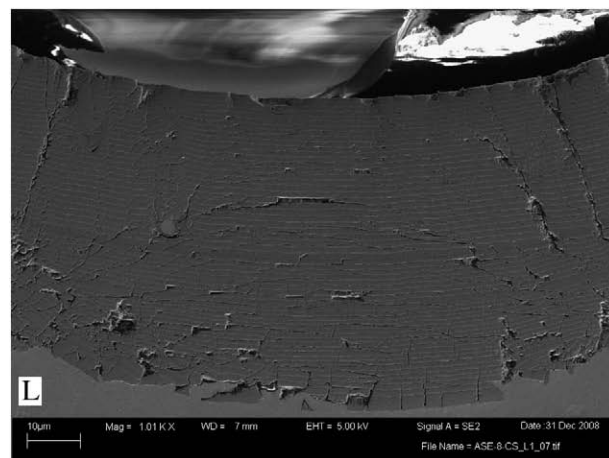
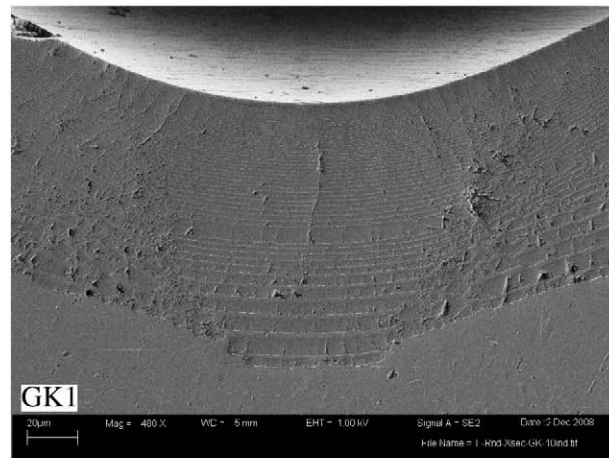


Fig. 6. SEM image of Rockwell indentation in nano-microlaminated two-segment coating  $GK_1$  (top) and TiAl/TiAlN nano-microlaminated coating I (bottom).

in larger columnar grain morphology. Larger columns may contribute to better fracture resistance in this ultra-thick ceramic coating.

The SEM images of Rockwell indentations in two nano-microlaminated coatings having smaller bi-periods,  $K_1$  with 40 bi-layers per 50  $\mu\text{m}$  coating thickness and  $K_2$  with 110 bi-layers per 12  $\mu\text{m}$  coating thickness (this coating was deposited on double rotating substrate) are shown in Fig. 4. It can be seen that coating  $K_1$  shows much better fracture resistance behavior than coating  $K_2$ . In the central area of indentation, where the compressive stress is maximum, the crack density in  $K_1$  coating is relatively low, while the crack pattern within the  $K_2$  coating resembles that of the monolithic coatings I and J. It shows that when the bi-layer period in multilayer Ti/TiN coatings and, especially the thickness of the metallic sublayers decreases to nanometric size its fracture behavior becomes similar to that of monolithic coatings.

Using laminated architectures with weak interlayers is a well-known strategy for toughening ceramics [8]. The microlaminated Ti/TiN coating G, having large ceramic layers separated by relatively large metallic layers, shows cracks that are largely confined to the ceramic layers as can be seen from Fig. 5. This behavior is similar for both  $K_1$  and G coatings and can be clearly seen in the indentation cross-section of the two-segment  $GK_1$  coating having bottom G segment and top  $K_1$  segment separated by a 5  $\mu\text{m}$  thick TiN interlayer as shown in Fig. 6 (top). It can also be seen that transverse cracks are developed within relatively thick ceramic TiN sublayers in the bottom coating segment G. These cracks may be explained by inter-columnar shear mode as suggested in [9]. Similar behavior can be observed in the TiAl/TiAlN nano-microlaminated coating, which shows mostly lateral and inclined cracks as illustrated in Fig. 6 (bottom). It can be seen from these indentation marks that these coatings experience all modes of fracturing, including lateral cracks, bending cracks, inclined cracks and transverse cracks possibly due to inter-columnar shear as was also found in a microindentation study in [9] for thick coatings on soft metallic substrates.

#### 4. Conclusions

The unidirectional dual arc LAFAD vapor plasma source has been characterized as a generator of high density ion current and mass flow for deposition of thick ceramic and cermet coatings in an industrial-scale batch coating system with exceptionally high deposition rates. The uniformity of the coating deposition rate can be controlled by a superimposed vertical rastering magnetic field. The LAFAD coatings are characterized by nearly defect-free morphology and by a smooth surface with an extremely low density of the growth defects that are typical in DCAD and magnetron processes, such as nodules, large

grain, voids and porosity. The hardness of ceramic and cermet coatings with thicknesses ranging from 20 to 100  $\mu\text{m}$  deposited by the LAFAD process ranges from 15–20 GPa for multilayer coating to 25 GPa for nano-microlaminated coatings to 35 GPa for monolithic ceramic coatings, while at the same time having extremely low stress levels. It was found that crack trajectories in ultra-thick laminated Me/MeN LAFAD coatings having relatively thick metallic interlayers are predominantly lateral, confined into the ceramic sublayers restricted by two neighboring metallic sublayers; but eventually they incline from the lateral to the transverse direction across the coating. On the other hand, when bi-layer thickness – specifically metallic sublayer thickness – is reduced to nanometric size, the crack development behavior becomes similar to that of monolithic coatings.

#### Acknowledgements

The author would like to acknowledge the technical assistance of Dave VanVorous for conducting the experimental trials, John O'Keefe for preparation of sample cross-sections and Chris Bowman for testing the mechanical properties. Thanks are also due to Recep Avci, Paul Gannon and John Wallace for carrying out the SEM analysis and Thomas Wittberg for coating composition analysis. Portions of this research were supported by the United States Department of Defense via Contract No. W911NF-05-2-0016.

#### References

- [1] Vladimir I. Gorokhovskiy, Rabi Bhattacharya, Deepak G. Bhat, Surf. Coat. Technol. 140 (2) (2001) 82.
- [2] R.L. Boxman, D.M. Sanders, P.J. Martin, Handbook of Vacuum Arc Science and Technology, Noyes Publications, Park Ridge, NJ, 1995.
- [3] V. Gorokhovskiy, C. Bowman, D. VanVorous, J. Wallace, Deposition of Various Metal, Ceramic and Cermet Coatings by an Industrial-Scale LAFAD Process, JVST A, 27 (4) (2009) 1080.
- [4] Ronghua Wei, Edward Langa, Christopher Rincon, James H. Arps, Deposition of thick nitrides and carbonitrides for sand erosion protection, Surf. Coat. Technol. 201 (2006) 4453.
- [5] Y.H. Cheng, T. Browne, B. Heckerman, J.C. Jiang, E.I. Meletis, C. Bowman, V. Gorokhovskiy, Internal stresses in TiN/Ti multilayer coatings deposited by large area filtered arc deposition, J. Appl. Phys. 104 (2008) 093502.
- [6] H. Kostenbauer, G.A. Fontalvo, M. Kapp, J. Keckes, C. Mitterer, Annealing of intrinsic stresses in sputtered TiN films: the role of thickness-dependent gradients of point defect density, Surf. Coat. Technol. 201 (2007) 4777.
- [7] K.J. Ma, A. Bloyce, T. Bell, Examination of mechanical properties and failure mechanisms of TiN and Ti-TiN multilayer coatings, Surf. Coat. Technol. 76–77 (1995) 297.
- [8] W. Lee, W.J. Clegg, The deflection of cracks at interfaces, Key Eng. Mater. 116–117 (1996) 193.
- [9] S. Bhowmick, R. Bhide, M. Hoffman, V. Jayaram, S.K. Biswas, Fracture mode transitions during indentation of columnar TiN coatings on metal, Philos. Mag. 85 (25) (2005) 2927.